Biotribology 19 (2019) 100101

Contents lists available at ScienceDirect

Biotribology

journal homepage: www.elsevier.com/locate/biotri

Distribution of the local required coefficient of friction in the shoe–floor contact area during straight walking: A pilot study

Takeshi Yamaguchi[a,b,*]

[a] Graduate School of Engineering, Tohoku University, 6-6-01 Aramaki-Aza-Aoba, Aoba-ku, Sendai, Miyagi 980-8579, Japan
[b] Graduate School of Biomedical Engineering, Tohoku University, 6-6-01 Aramaki-Aza-Aoba, Aoba-ku, Sendai, Miyagi 980-8579, Japan

ARTICLE INFO

Keywords:
Slip
Gait
Friction
Wearable sensor

ABSTRACT

We developed a shoe mounted with miniature tri-axial force sensors and investigated the distribution of the local required coefficient of friction (RCOF) in the contact area between the shoe sole and floor during straight walking. Four miniature force sensors were mounted on the outsole of the shoe. The study comprised five healthy young adult males (mean age: 22.4 years). Participants were instructed to walk straight at a normal pace on a level resin floor under 25 different sensor layouts to measure the three-directional ground reaction forces (GRFs) at 52 local positions in the region of the shoe sole. The local RCOF value (the maximum peak value of the ratio of the horizontal GRF to vertical GRF) was calculated at each sensor position. The mean local RCOF values at ten local positions were observed to be > 0.4, whereas those at the lateral rear foot and toe were observed to be > 0.6. These local RCOF values were much higher than the mean RCOF values calculated from the resultant local GRFs (0.18). The results of the present study will provide information on the distribution of friction requirements and the direction of applied horizontal GRF will aid in the development of slip-resistant shoe sole patterns.

1. Introduction

Slip-induced falls are one of the leading causes of occupational accidents [1,2]. A person is unlikely to slip if the ratio of the tangential force to the vertical force applied to the floor, i.e., the traction coefficient, is lower than the coefficient of friction at the shoe–floor interface during the stance phase. Further, the peak traction coefficients appear either shortly after weight acceptance or during push off [3], leading to increased slip risk. The peak traction coefficient observed shortly after weight acceptance during unperturbed walking is called the required coefficient of friction (RCOF) [4]. The RCOF is defined as the minimum coefficient of friction that is necessary at the shoe–floor interface to sustain human locomotion without slipping [5–9]. and it is used to predict the risk of hazardous forward slipping [10,11].

The tangential and vertical forces between the shoe and floor are typically measured as the horizontal ground reaction force (GRF) and vertical GRF, respectively, using a force plate [7–9]. However, GRFs are the net effects of multiple local forces that are acting across the entire contact area. Thus, it is difficult to obtain the distributions of local GRF and RCOF values in the entire contact area between the shoe and floor using the force plate. The distributions of local GRF and traction coefficient values in the shoe–floor contact area will provide information about the location in the contact area where a large coefficient of friction is required, and this will contribute to the development of slip-resistant shoe sole patterns. Moriyasu et al. [12,13] developed a shoe that was mounted with miniature tri-axial force sensors on the shoe outsole and measured the GRFs and traction coefficient at 19 local positions in the shoe sole area while running. However, there has been no study about the distributions of local GRF and traction coefficient values in the entire contact area between the shoe and floor during walking. Particularly, the GRF vector distribution and traction coefficient values shortly after weight acceptance and during push off, when the total shoe slip is likely to occur, should be understood while designing slip-resistant shoes. Further, the local slips in the contact area of the shoe sole can cause wearing of the tread block of the shoe outsole even when total shoe slip does not occur. Therefore, it is imperative to ascertain where the local slips are more likely to occur while developing a wear-resistant shoe outsole.

Thus, herein, we develop a shoe mounted with miniature tri-axial force sensors; using a shoe sensor system, we investigated 1) the distribution of the local traction coefficient in the shoe–floor contact area while walking straight, 2) the GRF and traction coefficient shortly after weight acceptance and during push off when slips are likely to occur to understand the relation between the risk of whole shoe slip and local

* Corresponding author at: Graduate School of Biomedical Engineering, Tohoku University, 6-6-01 Aramaki-Aza-Aoba, Aoba-ku, Sendai, Miyagi 980-8579, Japan.
E-mail address: yamatake@gdl.mech.tohoku.ac.jp.

https://doi.org/10.1016/j.biotri.2019.100101
Received 7 April 2019; Received in revised form 3 June 2019; Accepted 28 June 2019
Available online 29 June 2019

slip in the shoe–floor interface, and 3) the locations in the shoe–floor contact area at which local slips are likely to occur.

2. Methods

2.1. Shoe Device Mounted with Miniature Tri-Axial Force Sensors

To measure the local GRF distribution, four miniature tri-axial force sensors (ShokacChip, Touchence Inc., Japan) [14] were mounted on the shoe outsole. This sensor uses piezoelectric elements to detect three-dimensional forces. The size of each sensor was 11.1 × 11.1 × 2.5 mm, and the rate capacities in the x, y, and z directions, which correspond to the transverse ($+x$: lateral; $-x$: medial), longitudinal ($+y$: anterior; $-y$: posterior), and vertical directions of the shoe, were ± 10 N, ± 10 N, and 40 N, respectively (allowable overload: 150%). Four sensor devices with a backing made of steel plates (diameter: 9.0 mm, thickness: 0.5 mm), nitrile butadiene rubber (NBR) sheet (diameter:10.0 mm, thickness: 2.0 mm, hardness: 70 HS (A/15), 48 dummy devices, which included a rigid vinyl chloride plate (diameter: 10.0 mm, thickness: 3.0 mm), and NBR sheet (diameter: 10.0 mm, thickness: 2.0 mm), were attached to the bottom of a commercially available shoe (removed outsole), using double-sided tape (Fig. 1). The weight of the shoe with the sensor devices was approximately 350 gf (including the amplifier board connected to the shin). Of the four sensor devices, two were placed at fixed positions (i = 3 and 51 in Fig. 1) for each trial. The positions of the other two sensors were changed (25 sensor layouts), and GRF data from 50 local positions (i = 1, 2, 4–50, and 52 in Fig. 1) were collected. Thus, we acquired the three-dimensional GRF distributions of 52 locations. Because of the low rate capacity of the sensors, an NBR block was affixed at the heel of the shoe instead of the sensor devices.

2.2. Experimental Procedure

The study included five healthy young adult males. The mean (± standard deviation) age, height, and body mass were 22.4 ± 0.9 years, 1.67 ± 0.01 m, and 55.6 ± 3.1 kg, respectively. The participants were informed of the protocol, and informed consent was obtained from each participant prior to the experiment.

Participants wore the sensor shoe device on the right foot and wore a shoe mounted with 52 dummy devices on the left foot. The sensor amplifier board was fixed on the shank with a belt. Participants also carried a tablet personal computer for data collection on their back. They were instructed to walk straight for 30 steps at a self-selected normal speed on a level resin floor for each sensor layout. Therefore, 25 trials were performed per participant. In each trial, the GRF data of the right foot were obtained at a sampling frequency of 20 Hz, and the GRF data for 10 steps during the steady state were used for analysis.

Apart from the above gait trials, one of the participants was instructed to walk on a force plate (MG2060; Anima, Tokyo, Japan) placed at the center of a 5-m walkway, and GRFs obtained from the shoe device were compared to those obtained from the force plate. The participant was asked to walk at a self-selected normal speed, and 25 trials were performed with different sensor layouts to collect local GRF data for 52 sensor positions. The participant walked five times for each sensor layout condition.

2.3. Data Analysis

Heel contact (0% stance phase) and toe-off (100% stance phase) for each right foot step were determined using the vertical GRF f_{zi} for i = 3 (f_{z3}) and i = 51 (f_{z51}) with a threshold value of 2 N. GRF data were resampled to 26 points data from 0% to 100% stance phase at a 4% interval using Matlab (Mathworks, Natick, MA, USA). The local traction coefficient ϕ_i for each sensor position was calculated using the following equations:

$$\varphi_i = \frac{f_{hi}}{f_{zi}},\ i = 1\text{–}52 \tag{1}$$

$$f_{hi} = \sqrt{f_{xi}^2 + f_{yi}^2},\ i = 1\text{–}52 \tag{2}$$

where $f_{xi,}$ and f_{yi} are the GRFs in the transverse and longitudinal

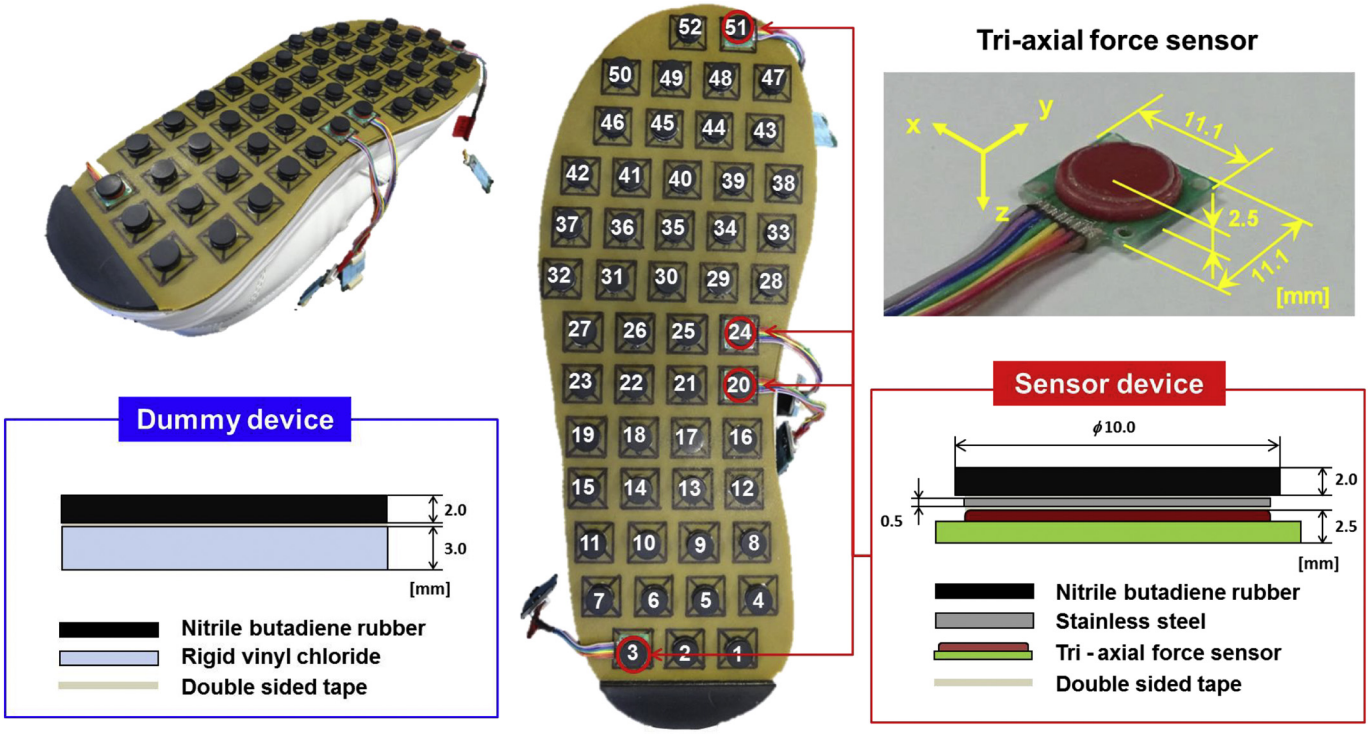

Fig. 1. Shoe device mounted with miniature tri-axial force sensors. In this sensor layout, sensor devices were placed at positions i = 3, 20, 24, and 51.

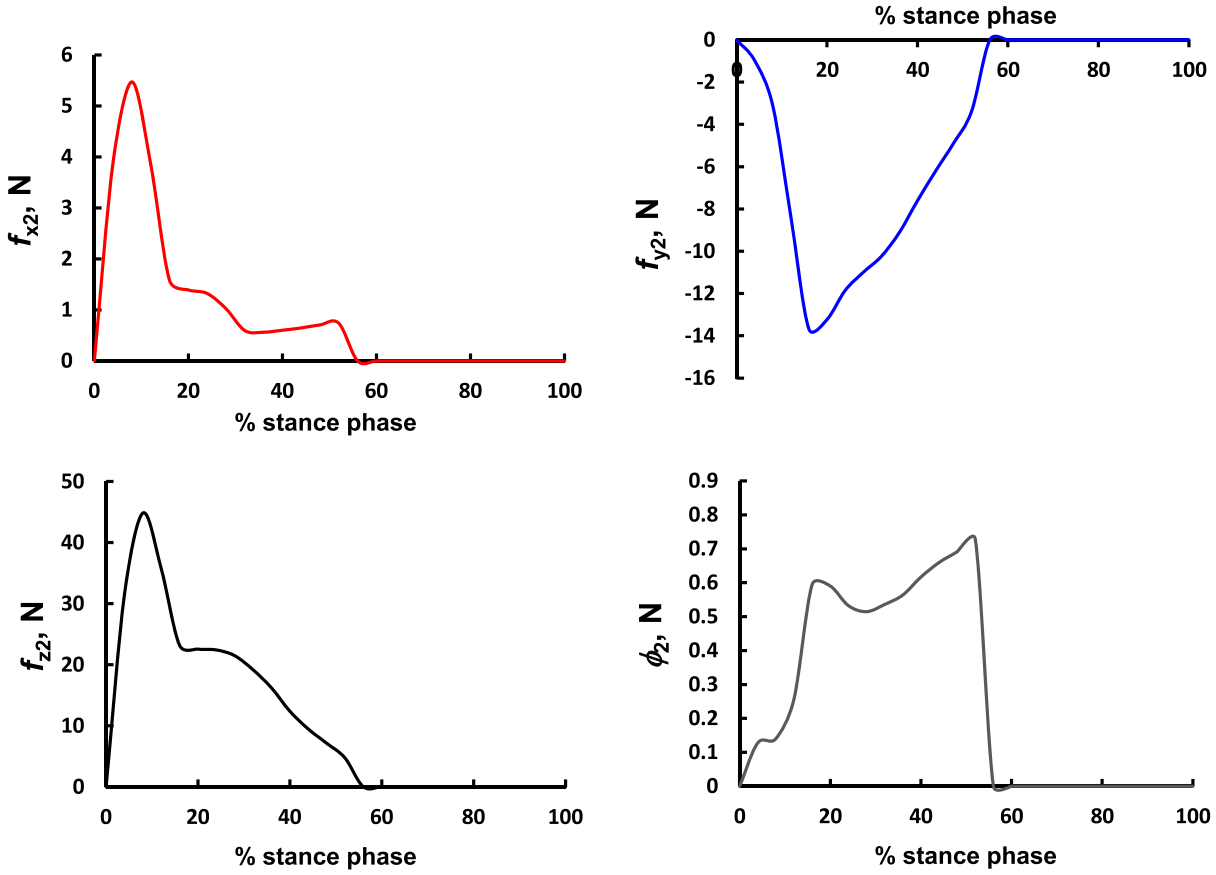

Fig. 2. The temporal profile of the local ground reaction forces (f_{x2}, f_{y2}, and f_{z2}) and local traction coefficient (ϕ_2) at rear foot (i = 2) for a single step in a single-participant experiment.

directions of the shoe, respectively, and f_{hi} is the resultant horizontal GRF at each sensor position. Fig. 2 depicts the temporal profiles of local GRF and traction coefficient when i = 2. The maximum value of the traction coefficient while the sensors experience contact with the floor at each sensor position was determined as the local RCOF value ($RCOF_i$). To screen data where instability in $RCOF_i$ occurred due to a small f_{zi}, we used the ϕ_i data at $f_{zi} > 5$ N in $RCOF_i$ determination. The resultant traction coefficient ϕ was calculated using the following equation:

$$\varphi = \frac{\sum_{i=1}^{i=52} f_{hi}}{\sum_{i=1}^{i=52} f_{zi}} \quad (3)$$

In the gait trials on the force plate, the sampling frequency of the force plate was 500 Hz, and the collected GRF data (F_x, F_y, and F_z) were low-pass filtered (10 Hz) with a fourth-ordered, zero-lag, Butterworth filter and then resampled to obtain 26 points data from 0% to 100% stance phase at a 4% interval using Matlab. The horizontal GRF (F_h) and vertical GRF (F_z) from the force plate were compared with the resultant horizontal and vertical GRFs ($\sum_{i=1}^{i=52} f_{hi}$ and $\sum_{i=1}^{i=52} f_{zi}$) obtained from the sensor shoe device at each stance phase. F_h was calculated using the following equation:

$$F_h = \sqrt{F_{x^2} + F_{y^2}} \quad (4)$$

3. Results

Fig. 3a shows the temporal profiles of the resultant horizontal and vertical GRFs obtained from the sensor shoe device and those obtained from the force plate. The temporal profiles of the resultant horizontal and vertical GRFs obtained from the sensor shoe device were in good agreement with those obtained from the force plate (Fig. 3a); however, the resultant vertical GRFs obtained from the sensor shoe device in the early stance phase, i.e., approximately 0–20% stance phase, were much smaller than those obtained from the force plate, possibly because of the lack of sensors at the heel of the sensor shoe. As shown in Fig. 3b, the resultant GRFs obtained from the sensor shoe device and the force plate were highly correlated with each other (r = 0.954, $p < .001$ for the horizontal GRF; r = 0.948, $p < .001$ for the vertical GRF). The slopes of the regression lines for the horizontal GRF and vertical GRF are 0.957 and 1.036, respectively. Further, the root mean square errors for the horizontal GRF and vertical GRF are 11.2 N and 57.5 N, respectively. These results indicate a relatively good accuracy of GRF measurement with the sensor shoe device.

The temporal profiles of local GRFs (f_{xi}, f_{yi}, and f_{zi}) for rear foot (heel, i = 2), midfoot (i = 27), and forefoot (metatarsal head, i = 43; toe, i = 49) in the gait trials on the resin floor are presented in Fig. 4. The peak values of the vertical GRFs were higher at the rear foot (f_{z2}) and metatarsal head (f_{z43}) than at the midfoot (f_{z27}) and toe (f_{z49}). Additionally, f_{y2} and f_{y27} were negative, which indicates that these forces acted as braking forces, while f_{y43} and f_{y49} were positive, which indicates that these forces acted as propulsion forces. Moreover, f_{x2}, f_{x27}, and f_{x49} were positive, which indicates that these forces were applied laterally, while f_{x43} were negative, which indicates that these forces were applied medially. The temporal profiles of the local traction coefficient (ϕ_i) for rear foot (heel, i = 2), midfoot (i = 27), and forefoot (metatarsal head, i = 43; toe, i = 49) are presented in Fig. 5. We discovered that the traction coefficients were higher at rear foot (ϕ_2) and toe (ϕ_{49}) when compared with those at the midfoot (ϕ_{27}) and metatarsal heads (ϕ_{43}). The traction coefficients at the midfoot (ϕ_{27}) and metatarsal head (ϕ_{43}) were low and stable during the whole contact period when compared with those at the rear foot (ϕ_2) and toe (ϕ_{49}).

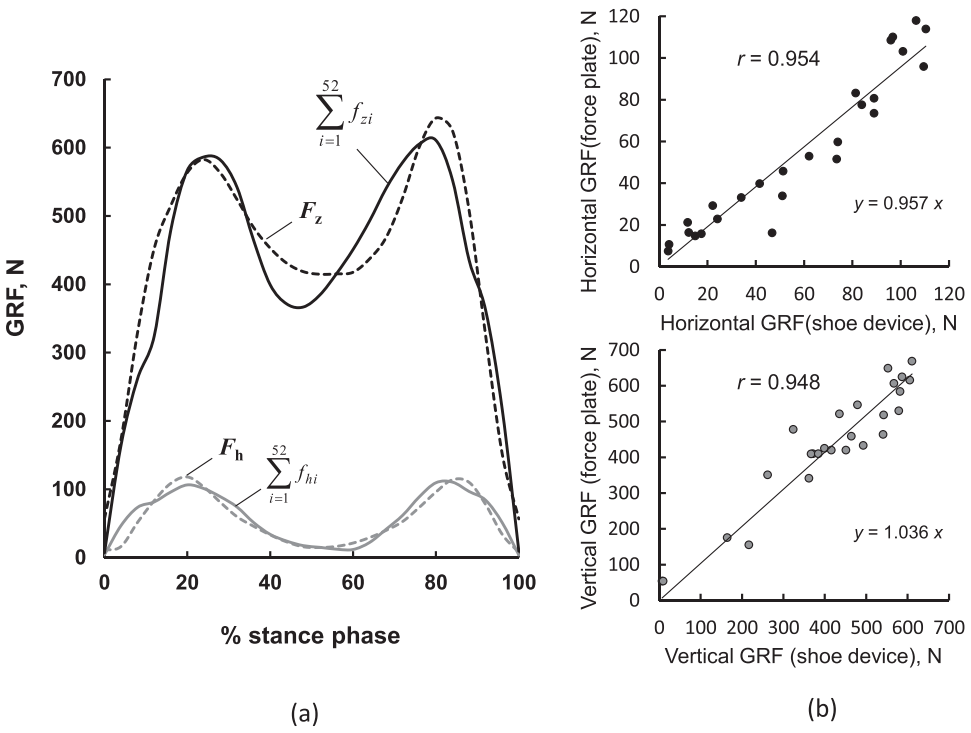

Fig. 3. (a) Temporal profile and (b) correlation of resultant ground reaction forces obtained using the sensor shoe device and the force plate. The GRF data from the force plate and the sensor shoe device at each stance phase (every 4% from 0% to 100%) is averaged across all the trials. The solid and dashed lines in (a) refer to the data obtained using the sensor shoe device and the force plate, respectively. The black and gray circles in (b) refer to the data obtained in the horizontal and vertical directions, respectively.

Fig. 6 shows the temporal profile of the resultant traction coefficient (Fig. 6a), and the magnitude of the local traction coefficient and direction of horizontal GRF, i.e., traction force, at each position in the 12% (i.e., shortly after weight acceptance), 52% (mid-stance), and 88% (terminal stance, i.e., during toe-off) stance phases (Fig. 6b). Fig. 7 represents the mean local traction coefficient at each sensor position in case of the 12%, 52%, and 88% stance phases. As shown in Fig. 6a, in the 12% stance phase, i.e., weight acceptance phase, the direction of horizontal GRFs was backward as a braking force in the entire contact area (Fig. 6a). At this instant, the local traction coefficient was higher at the lateral rear foot part (e.g., i = 2, 3, 7, 11, and 15) than at any other parts (Fig. 7a), and the horizontal GRFs at this area were backward and

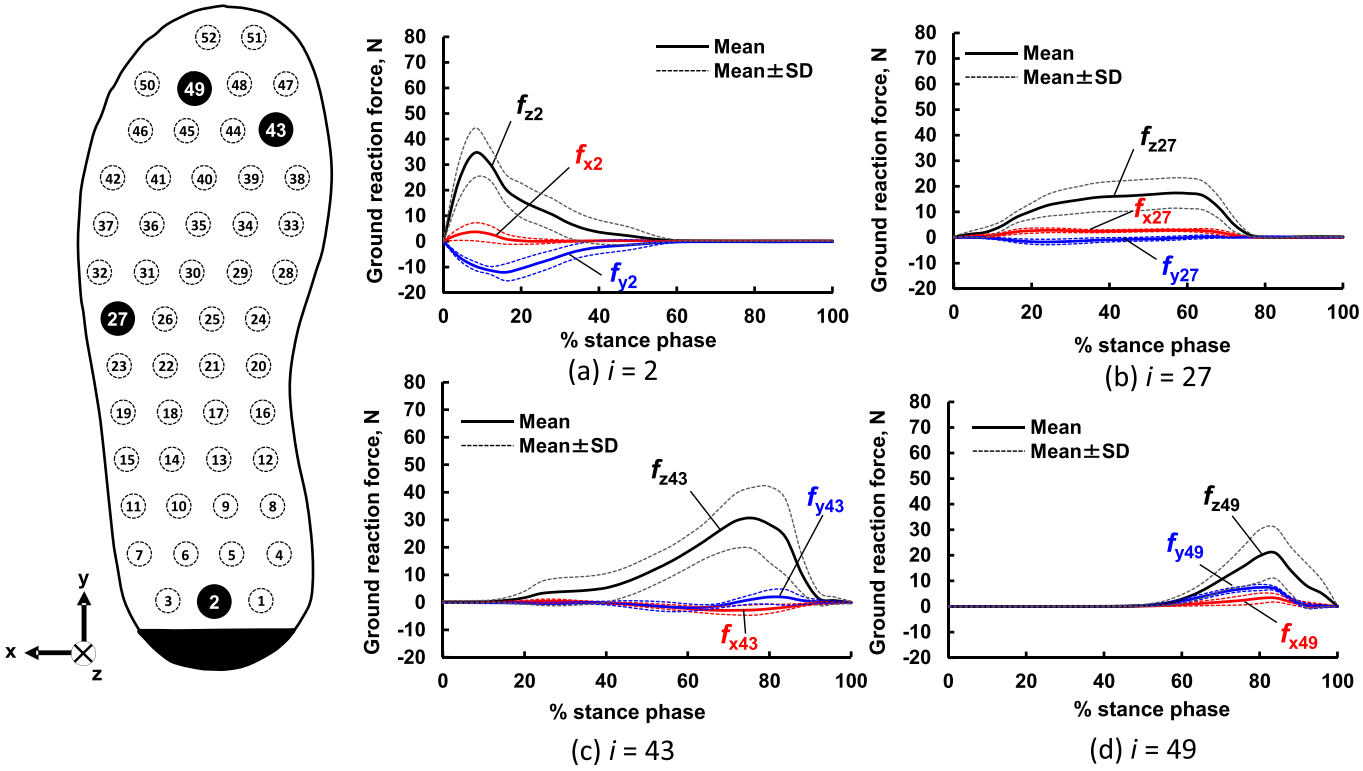

Fig. 4. Temporal profile of local ground reaction forces at the rear foot (i = 2), midfoot (i = 27), metatarsal head (i = 43), and toe (i = 49). The solid and dashed line indicate the mean value and mean ± standard deviation across all the subjects.

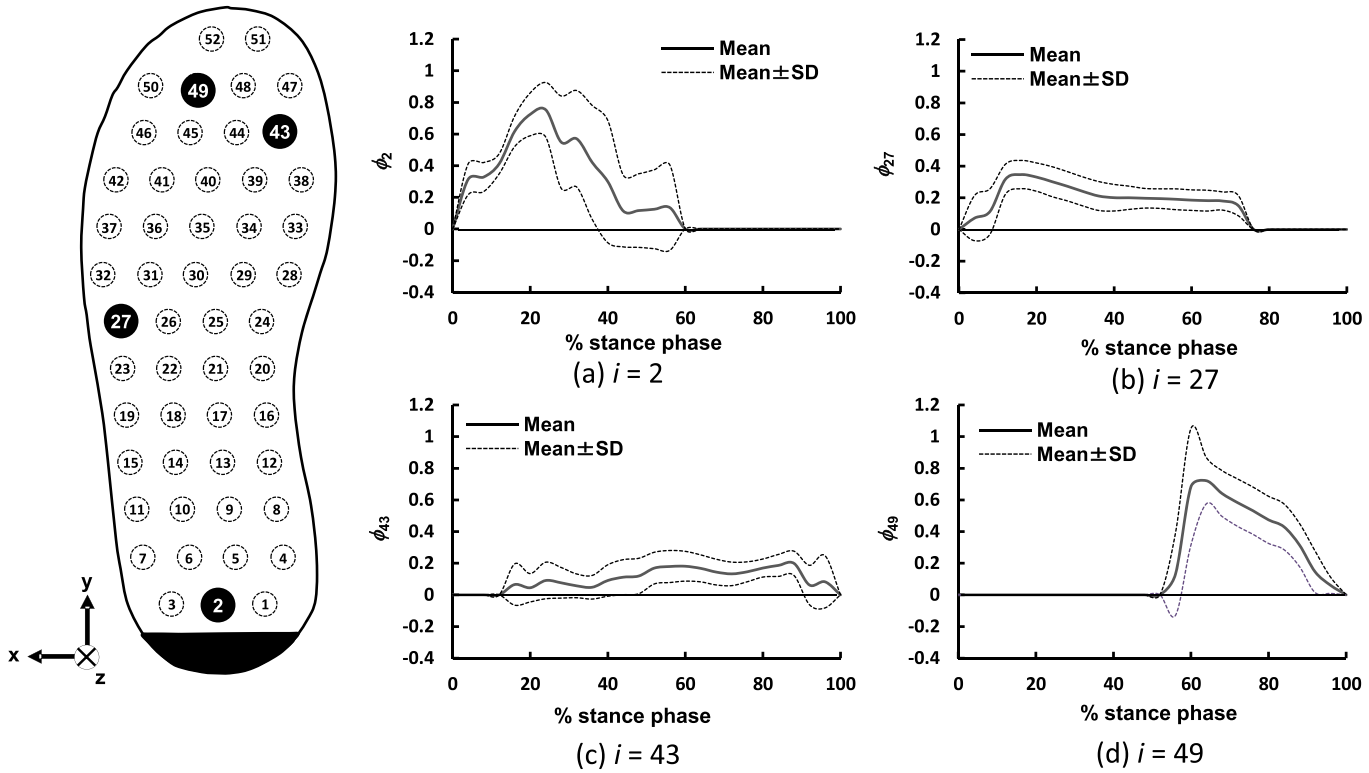

Fig. 5. The temporal profile of the local traction coefficient at the rear foot (i = 2), midfoot (i = 27), metatarsal head (i = 43), and toe (i = 49). The solid and dashed lines indicate the mean and mean ± standard deviation values for all the subjects, respectively.

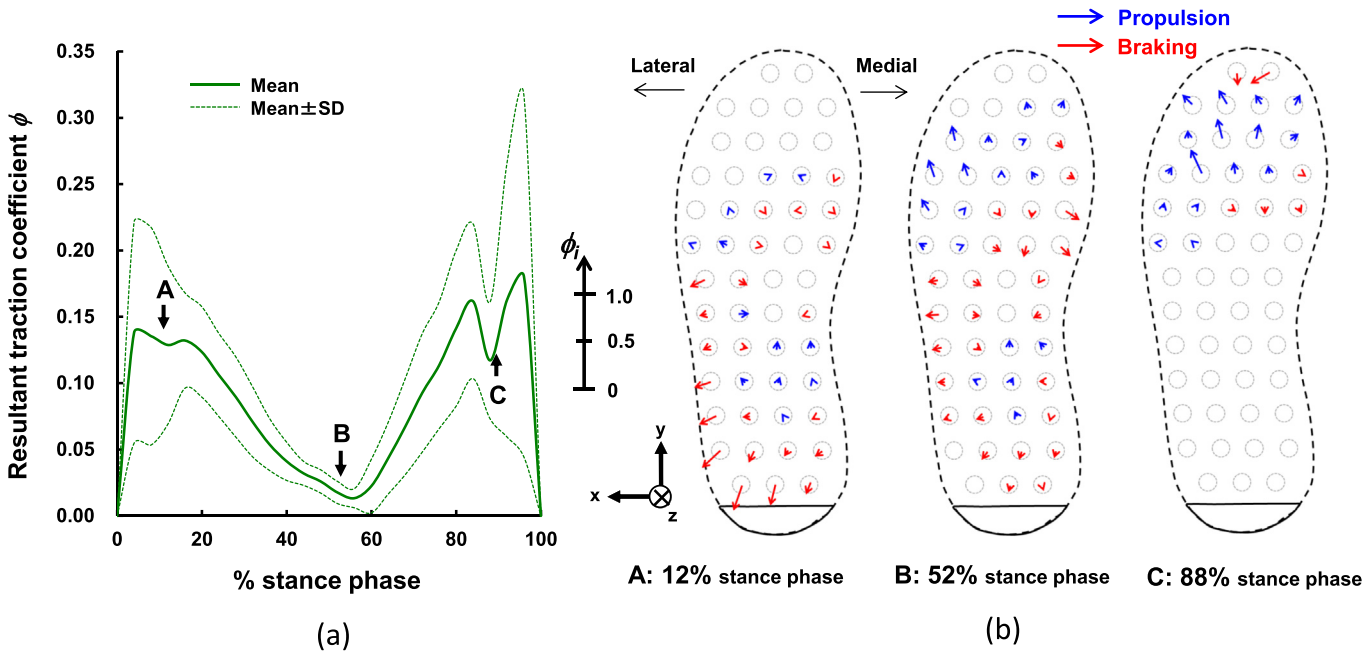

Fig. 6. (a) Temporal profile of the resultant traction coefficient and (b) the magnitude of the local traction coefficient and direction of the horizontal GRF at each stance phase. The data at each stance phase is averaged across all subjects. The length of the arrow in (b) indicates the magnitude of the local traction coefficient at each position. Red and blue arrows correspond to braking and propulsion, respectively. (For interpretation of the references to colour in this figure legend, the reader is referred to the web version of this article.)

lateral. On the other hand, in the 52% stance phase (Fig. 6b), the braking force and propulsion force were mixed in the contact area. These forces canceled each other, and therefore, the resultant traction coefficient at this instant was very low (0.018) as shown in Fig. 6a. In the 88% stance phase (Fig. 6c), the propulsion force was mainly applied at the metatarsal head and toe; however, the local traction coefficient in the forward and lateral directions at the lateral metatarsal head part and toe part (i = 41, 45, 49, and 50) was larger than the at any other part (Fig. 7c).

Fig. 8 shows the mean local RCOF value at each sensor position. It is

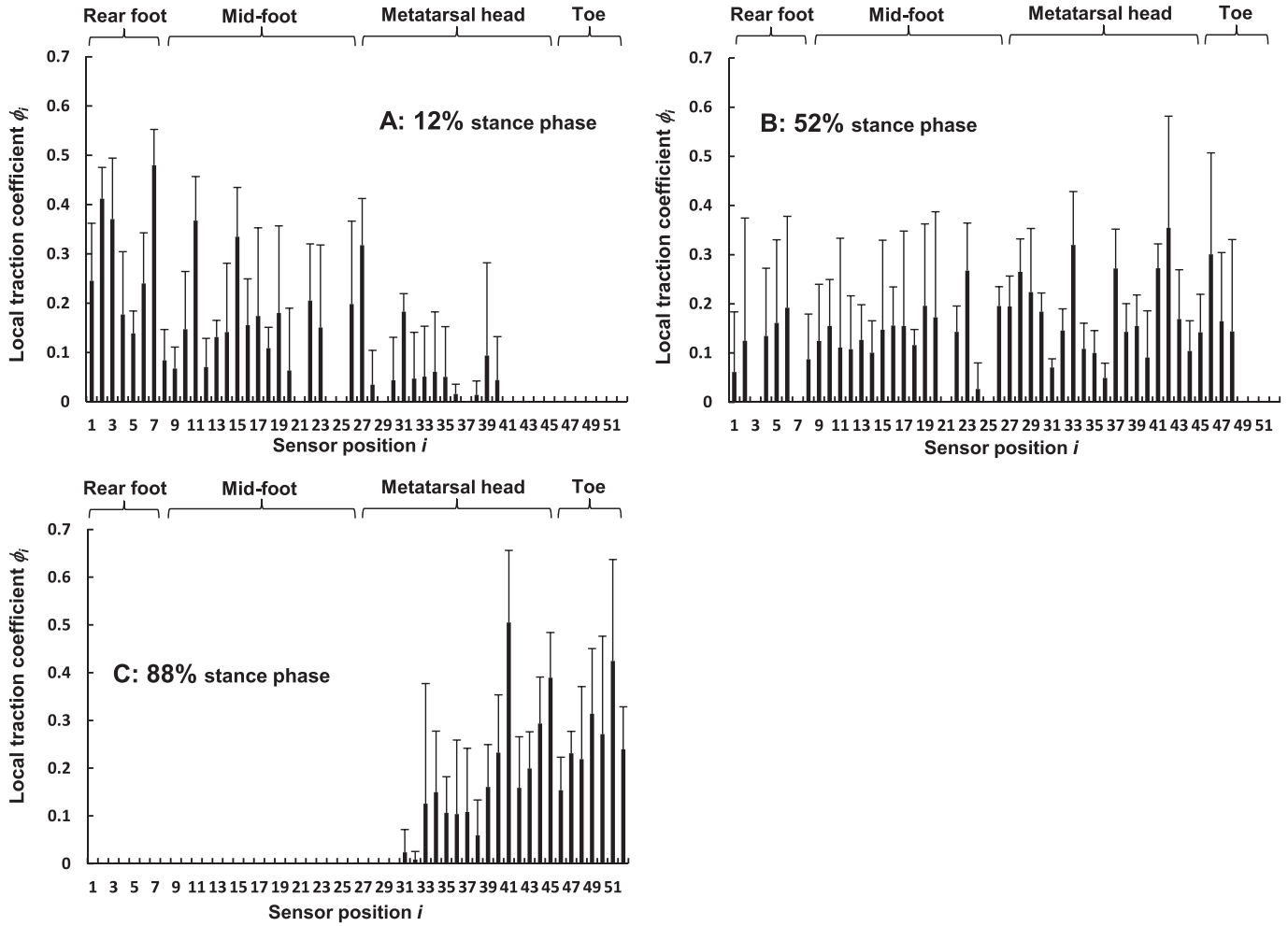

Fig. 7. Mean local traction coefficient values at each sensor position at each sensor position at 12% (loading response), 52% (mid-stance), and 88% (terminal stance) stance phase. Error bars indicate standard deviation among the five participants.

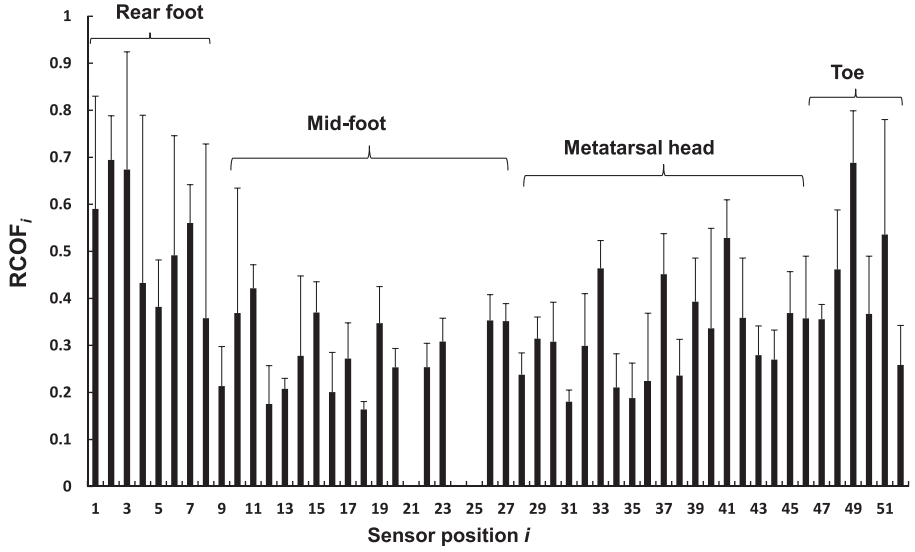

Fig. 8. Mean local required coefficient of friction ($RCOF_i$) values at each sensor position. Error bars indicate standard deviation among the five participants. There are no $RCOF_i$ data for the sensor positions 21, 24, and 25 (midfoot part) because the f_{zi} values at those sensor locations were less than the threshold value (5 N).

obvious that the local RCOF values vary depending on the location of the sole. It is obvious that the local RCOF values vary depending on the location of the sole. The mean local RCOF values at 10 local positions were > 0.4, and those at the lateral rear foot (i = 2 and 3), and toe (i = 49) were > 0.6.

4. Discussion

This study investigated the distributions of RCOF values in the contact area during straight walking, using a sensor shoe device. The obtained results denote that shortly after weight acceptance (e.g., the 12% stance phase), the local traction coefficient at the lateral real foot area is larger than the local traction coefficient experienced in the other areas when the resultant RCOF is large and whole slip is likely to occur. It is noteworthy that the local traction forces (horizontal GRFs) experienced at this area can be applied in the lateral backward direction. Thus, this area is likely to slip locally in the medial forward direction, and the friction loss in this region can propagate local slips to other tread block regions and result in total shoe slip. Additionally, during toe-off (e.g., the 88% stance phase), when the resultant RCOF is also large, the local traction coefficient at the head of the lateral metatarsal is still large; further, the local traction force at this area can be applied both in the forward and lateral directions. Thus, this area is likely to slip in the medial backward direction, which can propagate local slips to other tread block regions and lead to total shoe slip in the medial backward direction. However, at the mid-stance (e.g., the 52% stance phase), the resultant RCOF is small because of the local traction forces acting as propulsion and braking forces. Therefore, the local slip could occur in several directions, leading to the prevention of large global slips at the mid-stance phase. These results indicate why total shoe slip is likely to occur shortly after weight acceptance and during push off and not at mid-stance.

We found that the local RCOF values at almost the entire shoe–floor contact area were higher than the mean RCOF value (0.18) calculated using the resultant local GRFs obtained from Eq. (3). The results also indicated that the local RCOF values at 10 points mainly in the rear foot, metatarsal head, and toe area were larger than 0.4, which is believed to be preferable value to prevent global slip of the foot during walking [15–17]. However, global traction coefficient is not simply the sum of the local traction coefficient as shown in the following equation.

$$\varnothing = \frac{\sum_{i=1}^{n} f_{hi}}{\sum_{i=1}^{n} f_{zi}} = \frac{\sum_{i=1}^{n} \varnothing_i f_{zi}}{\sum_{i=1}^{n} f_{zi}} \neq \sum_{i=1}^{n} \varnothing_i \quad (5)$$

Therefore, the local traction coefficient is not directly related to the overall slip risk, and the friction coefficient does not need to be increased to the level shown in Fig. 8 to prevent global slipping. The local friction requirement relates to the local slip of an individual tread block of shoe sole. The increase in friction at an individual tread block results in increased overall friction in the shoe–floor interface. Therefore, the information of the distribution of friction requirement and the direction of the applied horizontal GRF will indicate where and in which direction the high slip-resistant tread blocks or grooves should be arranged. This information would also help in selecting the material for the shoe outsole. The distribution of local RCOF values at each sensor position can be a source of information about which part of the sole is likely to experience local slip. The local slips provide sliding wear of the tread blocks of the shoe sole. Therefore, the distribution of the local RCOF values denoted in Fig. 8 indicates that the rear foot and toe regions are likely to be worn because those regions experiences frequent local slips. This information can be utilized in the design to improve the wear resistance of the shoe sole.

We also investigated the direction of horizontal GRFs at each location in the contact area and found that the direction differed depending on the location. As shown in Fig. 6, horizontal GRFs were backward and lateral in the outer side of the heel in the early stance phase, which would be associated with external foot rotation at heel contact [18]. The direction can likely be affected by individual differences, sex differences, aging, and other such factors. When designing high slip-resistant outsoles for shoes, it is important to consider the direction of horizontal GRFs.

The present study had some limitations. We assessed straight walking in only five young adult males. Further studies are needed to investigate the generalizability of these results when considering females, elderly individuals, and impaired individuals, using a sensor shoe device. The lack of GRF data at the heel because of low sensor capacity limited the results of this study. Thus, miniature tri-axial force sensors with higher capacities should be developed to measure local GRF and local RCOF distributions in the entire shoe sole area.

5. Conclusion

In the current study, we developed a shoe mounted with miniature tri-axial force sensors and investigated the local RCOF at 52 local positions in the region of the shoe sole. Using a sensor shoe device, we determined the distribution of friction requirement and the direction of applied horizontal GRF during straight walking. The experimental results denote that shortly after weight acceptance and during toe-off at which the resultant RCOF is large and at which total shoe slip is likely to occur, the direction of traction force in which the traction coefficient is large is relatively uniform; thus, the resultant traction coefficient is large at these instances. However, at mid-stance, where the resultant RCOF is small and when total slip is not likely to occur, the directions of traction force in the contact area are different, resulting in the reduction of the resultant traction coefficient at that stance phase. The results also indicated that local RCOF values at most locations were higher than the RCOF values calculated from the resultant local GRFs (0.18). The local RCOF values at the lateral rear foot and toe were observed to be > 0.6, which was higher than those at the other sole region. Our results will contribute to the development of slip-resistant shoe sole patterns.

Acknowledgments

The authors would like to thank S. Takano and F. Meguro for their assistance. This work was partially supported by JSPS KAKENHI Grant Numbers 16K06038.

Conflict of Interest Statement

No author of this study has a conflict of interest, including specific financial interests, relationships, and/or affiliations relevant to the subject matter or materials included in this manuscript.

References

[1] T.K. Courtney, G.S. Sorock, D.P. Manning, J.W. Collins, M.A. Holbein-Jenny, Occupational slip, trip, and fall-related injuries can the contribution of slipperiness be isolated? Ergonomics 44 (2001) 1118–1137, https://doi.org/10.1080/00140130110085538.
[2] G.A. Koepp, B.J. Snedden, J.A. Levine, Workplace slip, trip and fall injuries and obesity, Ergonomics 58 (2014) 674–679, https://doi.org/10.1080/00140139.2014.985260.
[3] T. Yamaguchi, K. Hokkirigawa, 'Walking-mode maps' based on slip/non-slip criteria, Ind. Health 46 (2008) 23–31, https://doi.org/10.2486/indhealth.46.23.
[4] M.S. Redfern, R.O. Andres, The analysis of dynamic pushing and pulling; required coefficients of friction, Proceedings of the 1984 International Conference on Occupational Ergonomics I, 1984, pp. 573–577.
[5] P.J. Perkins, Measurement of slip between the shoe and ground during walking, in: C. Anderson, J. Senne (Eds.), ASTM STP 649. Walkway Surfaces: Measurement of Slip Resistance, ASTM, Philadelphia, 1987, pp. 71–87.
[6] L. Strandberg, H. Lanshammar, The dynamics of slipping accidents, J. Occup. Accid. 3 (1981) 153–162, https://doi.org/10.1016/0376-6349(81)90009-2.
[7] T. Yamaguchi, M. Yano, H. Onodera, K. Hokkirigawa, Kinematics of center of mass and center of pressure predict friction requirement at shoe-floor interface during walking, Gait Posture 38 (2013) 209–214, https://doi.org/10.1016/j.gaitpost.

2012.11.007.
[8] P. Fino, T.E. Lockhart, Required coefficient of friction during turning at self-selected slow, normal, and fast walking speeds, J. Biomech. 47 (2014) 1395–1400, https://doi.org/10.1016/j.jbiomech.2014.01.032.
[9] T. Yamaguchi, K. Masani, Contribution of center of mass-center of pressure angle tangent to the required coefficient of friction in the sagittal plane during straight walking, Biotribology 5 (2016) 16–22, https://doi.org/10.1016/j.biotri.2015.12.002.
[10] J.P. Hanson, M.S. Redfern, M. Mazumdar, Predicting slips and falls considering required and available friction, Ergonomics 42 (2009) 1619–1633, https://doi.org/10.1080/001401399184712.
[11] K.E. Beschorner, D.L. Albert, M.S. Redfern, Required coefficient of friction during level walking is predictive of slipping, Gait Posture 48 (2016) 256–260, https://doi.org/10.1016/j.gaitpost.2016.06.003.
[12] K. Moriyasu, T. Nishiwaki, T. Yamaguchi, K. Hokkirigawa, New technique of three directional ground reaction force distributions, Footwear Sci. 2 (2010) 57–64, https://doi.org/10.1080/19424281003685710.
[13] K. Moriyasu, T. Nishiwaki, T. Yamaguchi, K. Hokkirigawa, Experimental analysis of the distribution of traction coefficient in the shoe-ground contact area during running, Tribol. Online 7 (2012) 267–273, https://doi.org/10.2474/trol.267.
[14] ShokacChip™ Product Outline, Touchence Inc., 2019, http://www.touchence.jp/en/chip/index.html.
[15] H. Nagata, H. Watanabe, Y. Inoue, I.J. Kim, Fall and validities of various methods to measure frictional properties of slippery floors covered with soapsuds, Proceedings of the 17th World Congress on Ergonomics. Beijing, 2009 (CD-ROM).
[16] D.T.P. Fong, Y. Hong, J.X. Li, Human walks carefully when the ground dynamic coefficient of friction drops below 0.41, Saf. Sci. 47 (2009) 1429–1433, https://doi.org/10.1016/j.ssci.2009.04.005.
[17] T. Yamaguchi, T. Umetsu, Y. Ishizuka, K. Kasuga, T. Ito, S. Ishizawa, K. Hokkirigawa, Development of new footwear sole surface pattern for prevention of slip-related falls, Saf. Sci. 50 (2012) 986–994, https://doi.org/10.1016/j.ssci.2011.12.017.
[18] A. Chang, D. Hurwitz, D. Dunlop, J. Song, S. Cahue, K. Hayes, L. Sharma, The relationship between toe-out angle during gait and progression of medial tibiofemoral osteoarthritis, Ann. Rheum. Dis. 66 (2007) 1271–1275, https://doi.org/10.1136/ard.2006.062927.